INTERNATIONAL SOCIETY FOR
SOIL MECHANICS AND
GEOTECHNICAL ENGINEERING

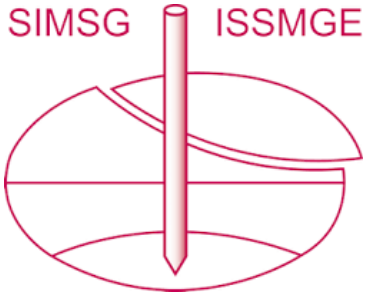

This paper was downloaded from the Online Library of the International Society for Soil Mechanics and Geotechnical Engineering (ISSMGE). The library is available here:

https://www.issmge.org/publications/online-library

This is an open-access database that archives thousands of papers published under the Auspices of the ISSMGE and maintained by the Innovation and Development Committee of ISSMGE.

The paper was published in the proceedings of the 6th International Conference on Geotechnical and Geophysical Site Characterization and was edited by Tamás Huszák, András Mahler and Edina Koch. The conference was originally scheduled to be held in Budapest, Hungary in 2020, but due to the COVID-19 pandemic, it was held online from September 26th to September 29th 2021.

Reconnaissance survey on earthquake-induced failures of ground composed of volcanic materials in Hokkaido, Japan, during the 2018 Hokkaido Eastern Iburi earthquake of *M*w=6.6

T. Hosoya
Chuo Kaihatsu Corporation, Tokyo, Japan, hosoya@ckcnet.co.jp

I. Towhata
Kanto Gakuin University, Yokohama, Japan, towhata.ikuo.ikuo@gmail.com

M. Ikeda
Chuo Kaihatsu Corporation, Sapporo, Japan, ikeda.mi@ckcnet.co.jp

ABSTRACT: The 2018 Hokkaido Eastern Iburi earthquake in Japan registered seismic magnitude of *M*w=6.6. The induced ground damage consists of two groups that are substantial slope failures in Atsuma Town and collapse of residential fill in Kiyota of Sapporo. Hill slopes in Atsuma is covered by many kinds of volcanic ash and pumice and the induced failures claimed 42 casualties. The authors studied those materials and obtained Yamanaka soil hardness which is quickly measured in situ. It was inferred that Tarumae volcanic pumice most likely developed shear failure, while the effect of heavy rain in the previous month is important as well. On the other hand, the damage in residential area in Kiyota was associated with liquefaction of volcanic filling materials, while decay of the fill quality is another issue. Same damage has been repeated during past earthquakes. Government quickly decided to repair this site by injection of colloidal silica with full financial support.

Keywords: earthquake, landslide, volcanic ash, soil hardness, case history

1. Introduction

The 2018 Hokkaido Eastern Iburi earthquake in Japan occurred at AM 3:08 at a focal depth of 37 km on September 6th and registered the moment magnitude of *M*w=6.6. Slope failure was the major cause of induced damage and 1631 houses were totally destroyed while 42 people were killed. The seismic intensity of JMA scale was the highest value of 7 in the epicentral area, which was consistent with the profound slope failures.

The induced damage was concentrated in two sites (Fig. 1). The first site of major damage is situated in Kiyota area in Sapporo (Fig. 2) which is approximately 55 km distant from the epicenter. The hilly terrain in Kiyota has been developed for residential purposes by filling volcanic materials in valley bottom. As is often the case in residential earth filling projects, the quality of fill is not very good unfortunately and liquefaction had occurred in Kiyota several times during past earthquakes. In 2018, the same problem was repeated in the same area. In particular, the foundation soil flowed away in Satodzuka District of Kiyota and the residential "land" disappeared.

The second site of damage is Atsuma Town in the epicentral area where a profound extent of failure occurred in many natural slopes (Fig. 3). The surface of the hills herein is covered by quaternary volcanic deposits (ash and pumice) that came from repeated eruption of several volcanos to the west. Because the volcanic materials deposited parallel to the slope surface, this mechanical weakness directly affected the slope

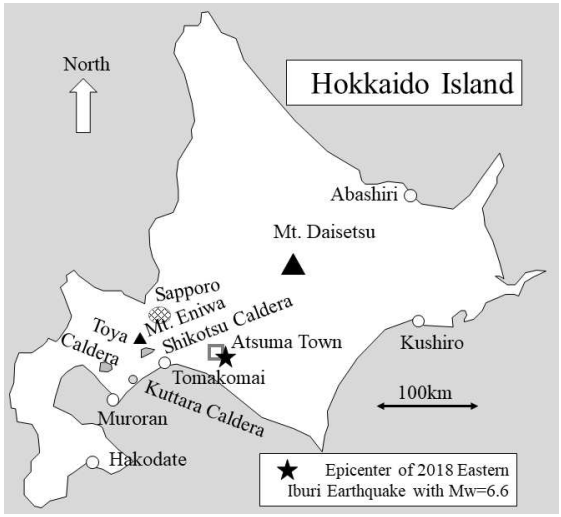

Figure 1. Map of Hokkaido Island showing important sites related with the 2018 Eastern Iburi earthquake.

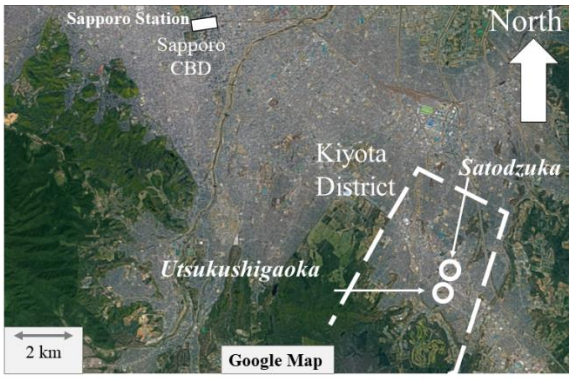

Figure 2. Location of Kiyota District in Sapporo City.

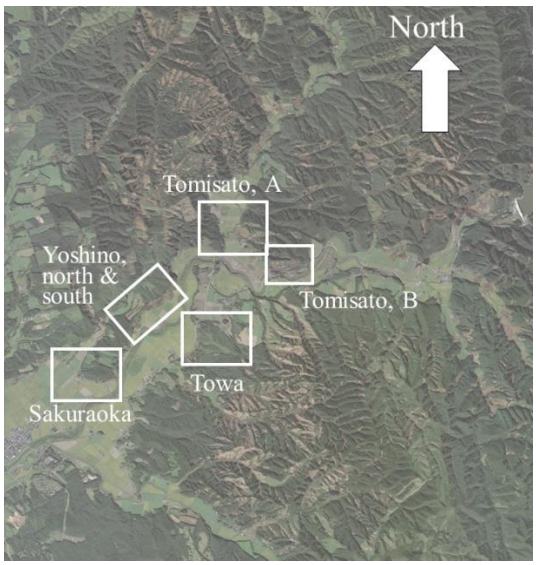

Figure 3. Areal view of Atsuma where many slope failure happened in volcanic deposits; brown color indicates the failed slopes (photograph provided by the Cabinet Office).

instability. The authors carried out field investigation in the volcanic ash slopes in order to shed light on the important roles of volcanic ash materials played in the observed slope failures. The present paper reports the results of field investigation and a brief analysis on the seismic stability of volcanic ash slopes.

2. *Seismic damage in Kiyota of Sapporo City*

The 2018 Eastern Iburi earthquake affected Sapporo City. Fig. 4 indicates the K-Net acceleration record at HKD180 station in Sapporo City. This station rests on a very thick soft soil and the maximum acceleration in EW direction was 153.5 cm/s^2, whereas the maximum value in the NS direction was 142.8 cm/s^2. The JMA seismic intensity in Sapporo was 5+ out of the maximum value of 7. When the earthquake happened, the first author was staying in Sapporo City for business and was able to immediately commence damage reconnaissance.

Figs. 5 and 6 illustrate the geotechnical damage in Satodzuka where residential land had been constructed in 1960s by filling former valleys with volcanic ash that was easily available in the vicinity. In the history of seismic damage, fills of volcanic ash have caused substantial damage; e.g., Sapporo [1] and Tsukidate in Miyagi [2]. During the present earthquake, a substantial amount of soil got fluidized and came out of the ground, leaving a big surface depression in the formerly level terrain. Fig. 7 shows an evidence of liquefaction of volcanic ash fill. Noteworthy is that liquefaction was repeated here, following the previous event during the 2003 Tokachi-oki earthquake that had magnitude of *M*w=8.0 but registered the JMA seismic intensity scale of only 4 in Sapporo City.

After this disaster, Sapporo Municipal Government initiated a quick response within 2018 towards restoration. The national governmnt had introduced a scheme for stabilization of disaster-prone slopes and the unstable ground in Satodzuka was decided to be restored from summer of 2019 by means of colloidal silica injection. The good point of this financial scheme is that all the expenditures are paid by the national government and the residents do not have to pay, although the affected land is their private property.

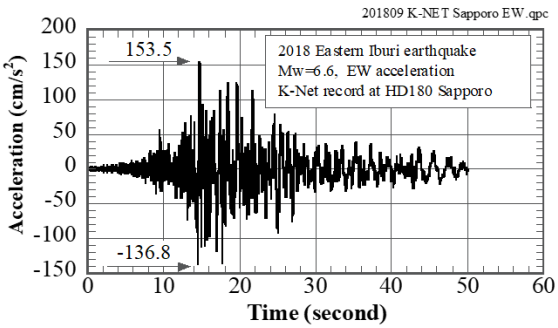

Figure 4. Acceleration record at K-Net HKD180 Station in Sapporo resting on thick soft subsoil.

Figure 5. Profound depression in fill part in Satodzuka, Kiyota, Sapporo.

Figure 6. Deposit of volcanic ash materials that flowed out of the fill (Satodzuka).

Figure 7. Sand ejecta in Utsukushigaoka area of Kiyota, showing repeated liquefaction after the previous event during the 2003 Tokachi-oki earthquake.

Note that the fundamental theme of the public sector states that damage in private property due to natural disaster should be restored by the owner's fund and that the public fund should not be spent on it. The recent trends, however, consider that ordinary people do not have knowledge on disaster mitigation. Therefore, the public sector attempts to provide financial supports to people as much as possible. As of November 2019, the restoration work is not completed. Although the progress of the work is faster than those after the 2011 gigantic Tohoku earthquake, it still needs time.

The ongoing discussion concerns the cause of the profound flow failure in Satodzuka (Figs. 5 and 6). Although liquefaction played some role in the disaster, additional discussion addresses possible deterioration of the earth fill structure, including walls and drainage channels. Much is not yet clear about these issues.

3. Slope disasters in Atsuma Town

In addition to artificial fills described in the previous chapter, natural slopes composed of volcanic ash are prone to seismic instability as well. Slope failures of this type in Central America are attributed to abrupt loss of grain interlocking and cementation during strong seismic loading [3]. Other examples of such a failure mechanism are the Las Colinas failure in El Salvador [4, 5], many slope failures during the 2009 Cinchona earthquake in Costa Rica [6, 7] and Mt. Ontake, Japan, in 1984 [8].

The hilly terrain in Atsuma Town is located to the east of several volcanos and calderas (Fig. 1) and the ground surface is covered by many strata of different volcanic materials. Table 1 summarizes the volcanic materials that are seen in the area. In the Holocene part, the existence of perched ground water has been recognized. Fig. 8 demonstrates the acceleration records obtained at JMA (Japanese Meteorological Agency) Atsuma Station and at K-Net Oiwake Station both of which are located very close to the epicenter (Fig. 1). While the maximum acceleration was strong in both positive and negative directions, they were short-term peaks and the remaining parts of the record were held within more or less 400-600 cm/s^2. Then the issue is the behavior and resistance of local deposit of volcanic ashes undergoing this earthquake motion.

Fig. 3 revealed that volcanic ash slope failed at numerous places in Atsuma. More details of slope failure are addressed in what follows. First, Fig. 9 illustrates that the slope failed rather uniformly in the horizontal direction, implying uniform topographical and geological/mechanical properties of the slope. Another point is the long run-off of the failed soil mass over the wet rice paddy. Some parts of the head scarp with dark color suggest humid soil conditions. Fig. 10 was taken in Tomisato of Atsuma and shows that the failed soil mass traveled along the level surface of paddy. Because the paddy still held water near the time of Autumn harvest, the shear strength of clay in the paddy floor was low and allowed long-distance run-off. Fig. 10 indicates that the failed mass traveled over a long distance in the horizontal direction because the travel route was on wet and soft mud in rice paddy. The local practice of agriculture maintains water in the paddy in this season and reduced the shear strength of the soil, making sliding easy above it. Fig. 11 shows the appearance of one of the head scarps where ground water was still coming out two days after the disaster. This water probably corresponds to the perched water (Table 1) that was produced by antecedent rainfalls (Fig. 12).

Table 1. List of strata of volcanic materials encountered in Atsuma (for location of source volcanos, refer to Fig. 1) [9].

Name	Symbol	Age (1000 years before present)	Typical thickness (cm) in Atsuma	Remarks
Organic soil	hm		5±	Not volcanic
Tarumae a, pumice	Ta-a	AD1739	10±	By eruption of Tarumae volcano
Andosol*	kb		15±	
Tarumae b, pumice	Ta-b	AD1667	20-30	By eruption of Tarumae volcano
Paektu Volcanic tephra	B-Tm	1.0	0-3	Mt. Paektu, North Korea – China
Andosol*	kb		20-30	
Tarumae c, pumice	Ta-c	2.5-3.0	5±	Perched ground water
Andosol*	kb		40-55	
Tarumae d, pumice	Ta-d	8-9	80-100	Perched ground water
Tarumae d, Lower loam	Ta-Lm			Impervious, Base of Holocene strata
Eniwa a, pumice	En-a	19-21	20-40	Perched ground water
Eniwa a, Lower Loam	En-Lm			Impervious
Shikotsu 1, pumice	Spfa-1	40-45	300-400	Submerged in water
Kuttara 1	Kt-1	≥43	150±	Submerged in water
Shikotsu 3 to 6, pumice	Spfa-3 to 6		<50	Impervious Spfa3: Kt-Tk Spfa4: Kt-3
Shikotsu 7 to 10, pumice	Spfa-7 to 10	>60	>200	
Kuttara 6 tephra	Kt-6	75-85	50±	
Aso** 4 ash	Aso-4	85-90	>15	
Toya tephra	Toya	112-115	>30	
Kutcharo-Haboro tephra	Kc-Hb	130±60	<10	

* Domestically called "Kuro boku" and is a product of decayed plants in volcanic ash area.
** Aso is a gigantic caldera in Kyushu Island.

(a) At JMA Atsuma Station

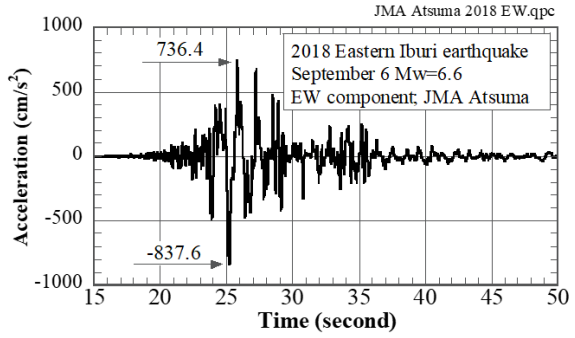

(b) At K-NET Oiwake Station

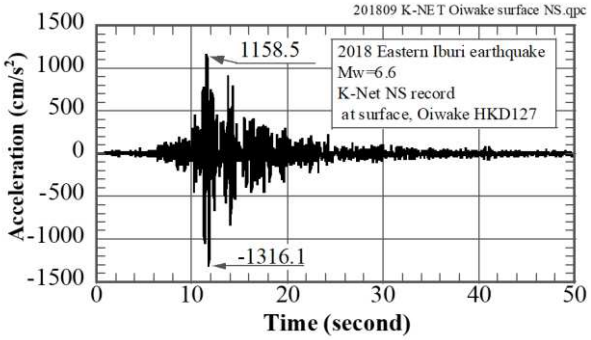

Figure 8. Acceleration records in and around Atsuma Town (out of EW and NS data, the stronger component was plotted at respective site).

Figure 9. Drone photograph of slope failure in Yoshino District of Atsuma Town.

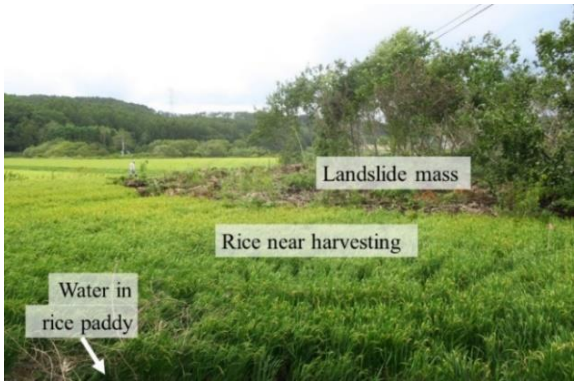

Figure 10. Landslide mass on soft rice paddy soil (Tomisato A District).

It is possible that the antecedent rainfall affected the slope instability. In this perspective, Fig. 12 presents the JMA rainfall record in Atsuma. The earthquake happened on the 37th day in this diagram. In 2018, the significant rainfall was recorded in mid August due to a typhoon. Afterwards, several precipitation events occurred. It appears that the amount of rainfall in 2018 did not signifi

Figure 11. Head scarp in Towa District (this photograph was taken on September 8th, 2018; two days after the disaster).

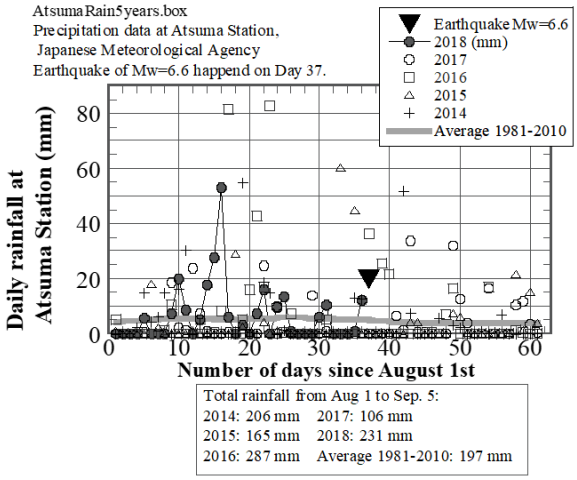

Figure 12. Rainfall records at JMA Atsuma Station in 2018 and in the past years.

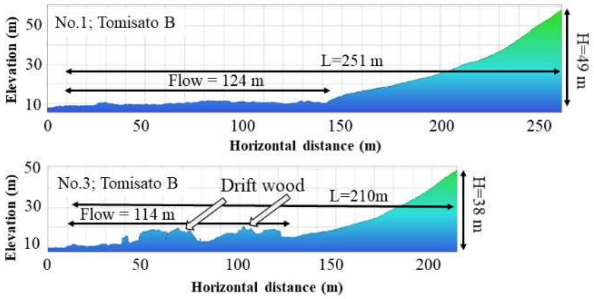

Figure 13. Cross sections of landslide mass in Tomisato B District.

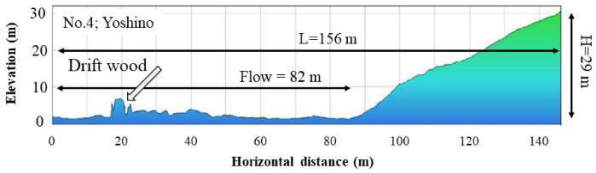

Figure 14. Cross section of landslide mass in Yoshino District.

-cantly exceed the previous years but was greater than the average trend for 1981-2010.

The geometric information on the landslide soil mass is discussed in what follows. The geometry was investigated by using drone photographs that were taken in Tomisato B and Yoshino Districts (Fig. 3). Fig. 13 shows two examples in Tomisato B District. The right ends of the figure are the place of top scarp. It is interesting that the distance of lateral flow exceeded the length of the source slope. This ease of flow was facilitated by soft paddy soil as stated above. Moreover, the shorter flow distance in No.3 of Tomisato is possibly the consequence of drift wood that increased the

frictional resistance over the paddy soil. Similar discussion is possible on Fig. 14 on failure in Yoshino District.

Table 2 summarizes the geometry of three studied failures. The ratio of flow distance vs. source length is nearly 1.0 or greater and implies the ease of flow on paddies. Another ratio was evaluated on the fall height (H) over the horizontal size (L); for their definisions, see Figs. 13 or 14. H/L is equal to $\tan\varphi_t$ where the friction angle [10] in terms of "total" stress is designated by φ_t. It is interesting that the obtained total-stress friction angle is uniformly equal to 10-11 degrees, irrespective of the different sizes and sites of slopes.

Table 2 Configuration of cross section of failed slopes.

Site	**No.1 Tomisato B**	**No.3 Tomisato B**	**No.4 Yoshino**
Flow distance (m)	124	114	82
Total horizontal length *L* (m)	251	210	156
Length of source = *L-Flow* (m)	127	96	74
Flow/Source	0.98	1.19	1.11
Fall height *H* (m)	49	38	29
H/L	0.20	0.18	0.19
Equivalent friction angle φ_t=arctan(*H/L*) (deg)	11	10	11

4. Field measurement of hardness of volcanic soils in Atsuma Town

Following the damage survey on September 6th and the following days, soil investigation was conducted urgently in Atsuma on September 23 and 24, 2018, which were 17 and 18 days after the earthquake. The investigation consisted of those on physical properties (grain size and Atterberg limits) as well as on shear strength of volcanic soils. It was not easy during this quick reconnaissance to conduct sounding (CPT etc.) or boring investigations in failed slopes. This difficulty comes mainly from lack of time and fund as well as the very unstable condition of failed soil mass. Due to this reason, the present study employed a simple equipment that is called Yamanaka Soil Hardness Tester [11]. Fig. 15 illustrates the concept of this equipment that consists of a small cone tip connected by a spring to a cylinder. It is small and can be brought to the top of unstable slopes. During field investigation, this equipment is placed on the surface of a slope (Fig. 16) and pushed into soil. Because the cylinder is held in contact with the soil surface, the penetration of cone is *40-x* (mm) in which the measured compression of the spring is *x* (mm).

The cone tip resistance per unit area, *P*, is assessed by using the spring deformation, *x*, as what follows. First,

$$Spring\ force = kx$$

where *k* is the elastic parameter of the spring. Second, because the length of the cone embedded in soil is *40-x* (mm), the cross section of the cone at the soil surface is given by $a(40-x)^2$ where *a* stands for the shape of the cone.

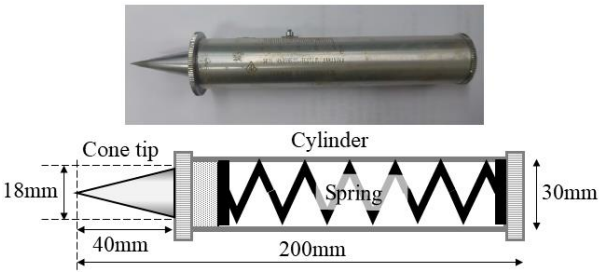

Figure 15. Schematic illustration of Yamanaka Soil Hardness Tester (Cone tip angle = 25.33 deg.; drawn after JGS Soil Testing Standard).

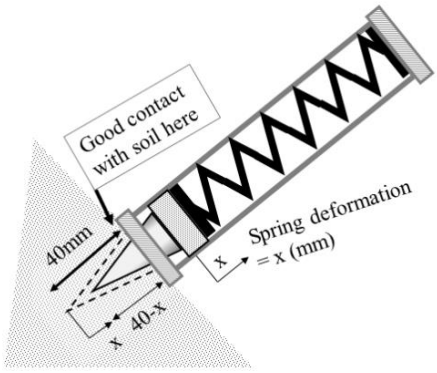

Figure 16. Use of Yamanaka Soil Hardness Tester at surface of slope

Hence, the force between the cone and the soil is given by $Pa(40-x)^2$. By equating this bearing capacity of the soil and the spring force, *P* is obtained as

$$P = \frac{kx}{a(40-x)^2} \quad (1)$$

where *k* and *a* are device-specific parameters as stated above.

Soil hardness was measured in several failed slopes. At each point of measurement, data was taken 3 times and the mean value was kept in record. First set of data was obtained in Sakuraoka District. Fig. 17 clearly shows layers of volcanic materials parallel to the slope surface. The depth of the slide was approximately 2m here. Fig. 18 illustrates the distribution of *P* value in the lower part of the side wall. Generally, the *P* value decreases as going downwards possibly because of inundation in perched ground water. In particular, the lower part of the Tarumae-d_2 pumice layer exhibits very low strength. Under this layer, a slip plane was encountered above the upper face of the underlying Tarumae loam layer (Ta-Lm) in which the *P* value was 79.5 kN/m^2 (Fig. 19). Thus, slip happened at the interface between the overlying weaker and underlying stiffer layers.

Fig. 20 illustrates the hardness test in the slip plane in Towa District where *P* value was found to be 50.0 kN/m^2. Noteworthy is that the *P* value above this position was 96.1-137.3 kN/m^2 that was greater than at the slip plane. This suggests again that slip happened at the bottom of a softer stratum resting on harder layer. Furthermore, the *P* value in the slip plane is within the range of 8 (Ta_{d2A}) -50 (Fig. 20) kN/m^2, although the variation of material properties is substantial. Table 3 shows physical properties of materials in Sakuraoka slope in which the loam at the bottom (Ta-Lm) is shown to be fine grained cohesive soil. It is, hence, reasonable to consider this layer impervious and capable of producing perched water above its level.

Figure 17. Overall view of a landslide site in Sakuraoka.

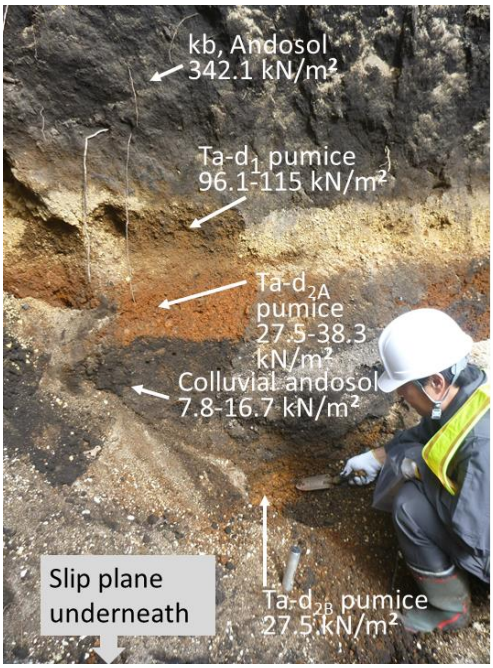

Figure 18. Soil Hardness in Sakuraoka instability site.

Figure 19. Yamanaka Soil Hardness Test immediately below the slip plane in Sakuraoka instability site.

Figure 20. Yamanaka Soil Hardness Test immediately below the slip plane in Towa instability site.

Table 3 Physical property of Tarumae Pumice and Lower Loam in Sakuraoka instability site.

Strata	**Ta-d_{2A}**	**Ta-d_{2B}**	**Ta-Lm**
Specific gravity of soil grain, G_s (g/cm^3)	2.527	2.509	2.672
Fines content (%)	16.2	21.7	78.1
Mean grain size, D_{50} (mm)	1.4	1.4	**0.016**
Uniformity coefficient, U_c	69.65	173.99	---
Natural water content (%) 17-18 days after the disaster	150.2	279.1	30.5
Liquid limit (%)	191.1	NP	47.6
Plastic limit (%)	102.3	NP	24.8

5. Assessment of undrained shear strength of volcanic deposits

This chapter makes an attempt to assess the undrained shear strength of soils, c_u, in several manners. In the first approach, the measured P value is considered to be the bearing capacity of a shallow foundation without embedment. Because the point of interest is the undrained strength of cohesive soil, the friction angle is set equal to zero. In this situation, the classical bearing capacity theory assumes

$$P=c_u N_c \quad (2)$$

where N_c is called a bearing capacity factor.

Geotechnical engineering practice adopts N_c=5.7 on the basis of Terzaghi's study. Because Terzaghi's study "somehow" hypothesized a realistic failure mechanism, this solution is an upper bound. An extremely simple failure mechanism as illustrated in Fig. 21 gives $N_c=2\pi=6.28$.

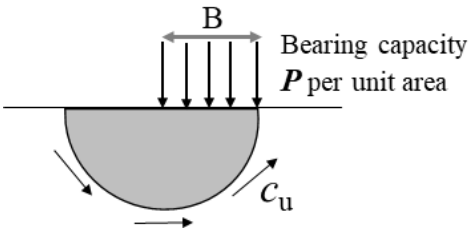

Figure 21. Circular failure mechanism hypothesized for simple calculation of N_c.

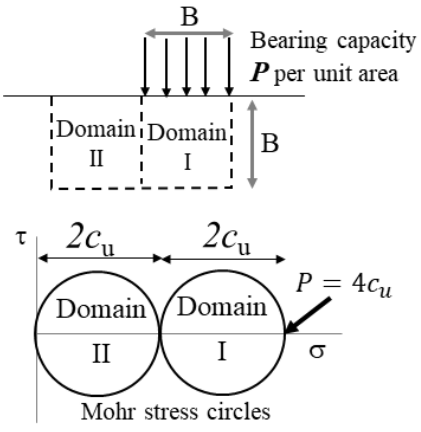

Figure 22. Simplified stress analysis on bearing capacity.

Second, a theoretical study obtained $N_c=\pi+2=5.14$ [12]. Because his study employed the calculation of force equilibrium in the subsoil, this solution is a lower bound.

Another very simple stress analysis (Fig. 22) gives *N*c=4 which is a lower bound.

The third approach is made of the equilibrium of forces acting on the cone (Fig. 23). Herein, the shear stress on the surface of the cone is considered to be the undrained strength, c_u. Because the shear force on the cone surface is in equilibrium with the pushing force, $P\times$(Bottom area of cone), Fig. 23 gives

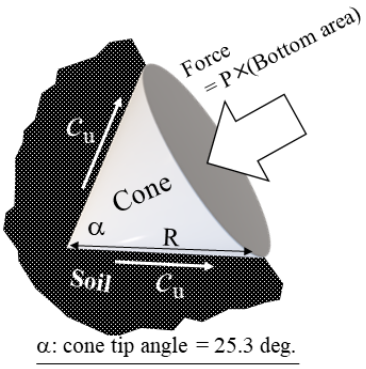

Figure 23. Force equilibrium between cone-surface shear stress and pushing force of soil hardness tester.

$$c_u \pi R^2 sin\frac{\alpha}{2} cos\frac{\alpha}{2} = P\pi \left(Rsin\frac{\alpha}{2}\right)^2 \text{ or}$$
$$c_u = Ptan\frac{\alpha}{2} \quad (3)$$

in which α stands for the cone tip angle and is equal to 25.33 deg. Therefore, Eq. 3 becomes

$$c_u = 0.225\ P \quad (4)$$

This implies Nc=1/0.225≅4.5 and is equivalent to the lower-bound values shown above.

By summarizing the three types of calculation, *N*c appears to be 5 to 6 and is reasonably assumed to be 5.5 without significant error.

Thus, c_u is suggested to be in the range of P/(Nc=5.5) that varies from 1.5 to 9.1 kN/m^2. Note that this value of strength may be an underestimation of the in-situ strength during the earthquake disaster because, when hardness tests were run, the tested soil likely had swelled after removal of the landslide mass and with ample supply of ground water (Fig. 11). Another reason for underestimation is the lack of overburden during hardness tests.

Preliminary stability analyses with c_u = 1.5 to 9.1 kN/m^2 gave very low factor of safety and need was felt to justify a greater value of soil's shear strength. Because no further information is available on in-situ strength when the present reconnaissance was conducted, the strength was increased in calculation by simply considering the effective stress produced by the weight of overburden landslide mass that had been lost during the Yamanaka hardness tests. This strength increment is given by

$$Strength\ increment = \sigma' tan\varphi \quad (5)$$

in which σ' stands for the effective stress normal to the slip plane and is given by

$$\sigma' = (\rho g - \rho_w g) h cos^2\theta \quad (6)$$

where ρg and $\rho_w g$ are unit weights of soil and water, and are equal to 17 and 9.8 kN/m^3, respectively. By substituting φ = 30 deg. and h = 2m, the strength increment is obtained to be 6.2 kN/m^2. Accordingly, 9.1+6.2=15.3 kN/m^2 is one of the possible strength values.

It is also possible to assess the in-situ strength by using φ_t = arctan*(H/L)* in Table 1. By taking this total-stress friction angle to be 11 deg., the shear strength is obtained as

$$\sigma tan\varphi_t = \rho g h cos^2\theta tan\varphi_t = 5.8 \text{ kN/m}^2 \quad (7)$$

In summary, the stability analyses will be carried out by using the strength values of 1.5, 5.8 by *H/L*, 9.1 and 15.3 kN/m^2.

6. Seismic stability analyses

A simple pseudo-static stability analysis is made in this chapter on a one-dimensional slope model shown in Fig. 24. The slope angle (θ) was set equal to 20 degrees, the soil thickness (h) was 2m, the unit weight of soil (ρg) was 17 kN/m^3, the seismic coefficient of a variety of range was given parallel to the slope surface for simplicity and the ground water level was located at the slope surface. The pseudo-static factor of safety is given as

$$F_S = \frac{c_u}{\rho g h cos\theta (sin\theta + K)} \quad (8)$$

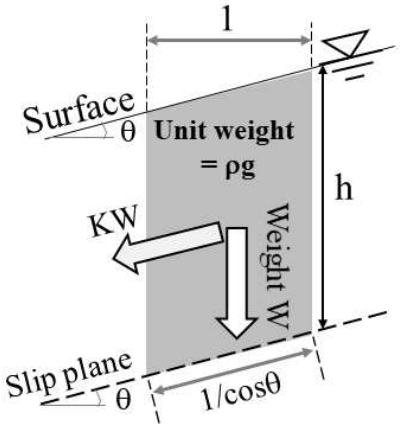

Figure 24. Stability analysis on infinite slope.

Fig. 25 illustrates the calculated factor of safety that varies with the value of seismic coefficient. The smaller values of c_u=1.5 and 9.1 kN/m^2 failed to give factor of safety greater than unity even under static conditions. c_u =5.8 kN/m^2 as assessed by *H/L* gave very small factor of safety as well. This is probably because the assessed strength corresponds to the state of flow which occurs after large distortion of soil. In other words, this strength corresponds to the residual strength after the peak strength has been achieved and softening has occurred.

In contrast, the preset study with c_u=15.3 kN/m^2 is able to demonstrate a possibly realistic factor of safety, which is greater than unity under static condition and becomes less than unity under some value of seismic coefficient, *K*. Although it is difficult to determine a particular value of *K* that is relevant to the measured maximum acceleration (*PGA*) in Fig. 8, an empirical formula on the

basis of seismic damage case histories of harbor strucutres may be useful [13];

$$Equivalent\ K=\frac{1}{3}\left(\frac{PGA}{g}\right)^{1/3} \quad (9)$$

where g stands for the gravity acceleration. This formula suggests *PGA*s in Fig. 8 to be equivalent to K=0.32 and 0.37. For this range of seismic coefficient, c_u=15.3 kN/m^2 gives the factor of safety less than unity, being consistent with the observed slope failure. Note further that c_u=5.8 kN/m^2 was obtained from *H/L* of failed slopes without considering the seismic inertial force. Therefore, the plot for this c_u value is reasonable only for $K=0$ which is indicated by a bigger triangle (▽) in the figure. Then, the factor of safety=0.53 at $K=0$ is not unrealistic for the seismically failed slopes.

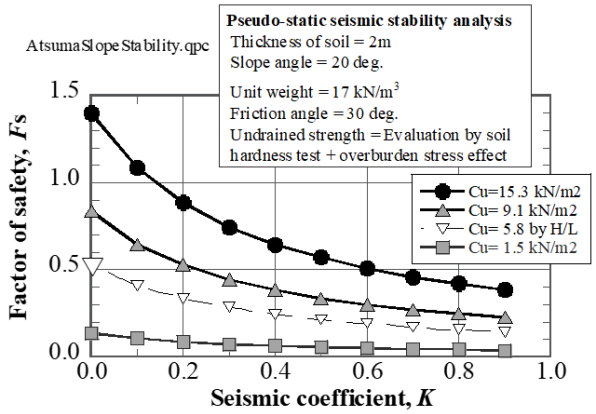

Figure 25. Seismic factor of safety varying with pseudo-static seismic coefficient.

7. Conclusion

After the 2018 Eastern Iburi earthquake of Mw=6.6 in Hokkaido, Japan, damage reconnaissance and soil investigation were conducted in the affected area. The major conclusions drawn from this study are shown in what follows.

(1) Residential area developed by cutting and filling volcanic ash materials in hilly terrain is prone to seismic liquefaction.

(2) Possibly, the deterioration of fill may have affected the stability of the residential fill.

(3) Natural slopes composed of volcanic ash deposits are seismically unstable.

(4) Antecedent rainfall probably produced perched ground water and affected the seismic stability.

(5) Yamanaka soil hardness tester is a portable device to measure the mechanical property of subsoil. It exhibited that slope failed at the bottom of soft volcanic deposits below which the shear strength suddenly increases.

(6) It is not easy, however, to determine the shear strength quantitatively. The measured strength appears underestimation.

(7) The reasons for underestimation are lack of overburden during measurement as well as soil swelling under the effect of rain water.

(8) In the slope instability analysis, the effect of overburden was added to the assesed strength and then the calculated factor of safety became realistic to a certain extent. Obviously, further study is needed in this respect.

References

[1] Kitago, S. and Toki, S. "Geotechnical investigation on the settlements of volcanic ashes and sand fills caused by the 1968 Tokachi-oki earthquake", Report on the Tokachi-Oki earthquake 1968, Special Committee for the Investigation of the Tokachi-Oki earthquake 1968: 463-494 (in Japanese), 1968.

[2] Joint Delegation of Japan Society of Civil Engineers and Japanese Geotechnical Society "Reconnaissance Report on the May 26, 2003 Miyagiken Oki earthquake", pp.9-13 (in Japanese), 2003.

[3] Bommer, J.J. and Rodriguez, C.E. "Earthquake-induced landslides in Central America", Engineering Geology 63: 189-220, 2002.

[4] Bommer, J.J., Benito, M.B., Ciudad-Real, M., Lemoine, A., López-Menjívar, M.A., Madariaga, R., Mankelow, J., De Hasbun, P.M., Murphy, W., Nieto-Lovo, M. and Rodríguez-Pineda, C.E. "The El Salvador earthquakes of January and February 2001: context, characteristics and implications for seismic risk", Soil Dynamics and Earthquake Engineering, 22, 389-418, 2002.

[5] Konagai, K., Johansson, J., Mayorca, P., Yamamoto, T., Miyajima, M., Uzuoka, R., Pulido, N.E., Duran, F.C., Sassa, K. and Fukuoka, H. "Las Colinas landslide caused by the January 13, 2001 off the coast of El Salvador earthquake", Journal of Japan Association for Earthquake Engineering 2(1), 1-5, 2002.

[6] Aoyama, S., Towhata, I., Vargas-Monge, W., Yasuda, S. and Goto, S. "The report about the landslide in Costa Rica Cinchona earthquake 2009", Proc. 40th National Conference of Japan Landslide Society, Niigata, pp. 189-190 (in Japanese), 2009.

[7] Barrantes-Castillo, G., Jiménez-Campos, C. and Ocón-García, M.J. "Deslizamientos provocados por el terremoto de Cinchona de 2009, Costa Rica", *Revista Geográfica de América Central*, *2*(51), pp.89-100 (in Spanish), 2013.

[8] Ishihara, K., Hsu, H.L., Nakazumi, I. and Sato, K. "Analysis of landslides during the 1984 Naganoken-Seibu earthquake", Proc. Int. Symp. Geol. Problems in Seism. Areas, Bari, Italy, pp. 175-215, 1986.

[9] Machida, H. and Arai, F. "Atlas of Tephra in and around Japan", Univ. Tokyo Press, ISBN978-4-13-060745-2, p. 336, 2003 (in Japanese).

[10] Hsü, K.J. "Catastrophic debris streams (Sturzstroms) generated by rockfalls", Geological Society of America Bulletin 86: 129-140, 1975.

[11] Yamanaka, K. and Matsuo, K. "Study on soil hardness I: relationship between soil hardness and moisture content", Soil Science and Plant Nutrition, 33(7): 343-347 (in Japanese) 1962.

[12] Prandtl, L. "Über die Härte plastischer Körper", Nachrichten von der Gesellschaft der Wissenschaften zu Göttingen, Mathematisch-Physikalische Klasse: 74-85 (in German), 1920.

[13] Noda, S., Uwabe, T. and Chiba, T. "Relation between seismic coefficient and ground acceleration for gravity quaywall", Report of the Port and Harbor Research Institute, 14, 67-111 (in Japanese), 1975.